applied sciences

MDPI

Article

Design Approach for Composite Pavement Structure Incorporating Reflective Crack Considerations

Naren Fang [1,2], Xuesen Wang [1], Huanyu Chang [3,*] and Kang Yu [4]

[1] School of Civil Engineering, Tianjin Chengjian University, Tianjin 300384, China; 2017021044@chd.edu.cn (N.F.); 15738606147@163.com (X.W.)
[2] Tianjin Key Laboratory of Civil and Structure Protection and Reinforcement, Tianjin 300384, China
[3] Academy of Eco-Civilization Development for Jing-Jin-Ji Megalopolis, Tianjin Normal University, Tianjin 300387, China
[4] No. 6 Engineering Co., Ltd. of FHEC of CCCC, Tianjin 300451, China; dqjys1988@163.com
* Correspondence: changhuanyu@tjnu.edu.cn; Tel.: +86-022-2308-5083

Abstract: The current design methods employed for composite pavement structures predominantly rely on cement concrete slabs, which unfortunately lack established design standards and associated control indicators for determining the appropriate thickness of the asphalt layer. Therefore, the emergence of reflective cracks at the bottom of the asphalt layer has become a prevalent issue in composite pavement. This article aims to enhance the existing design methodology for composite pavement structures by proposing the inclusion of "cracking at the bottom of the asphalt layer" as a design indicator. An extensive analysis was conducted to assess the influence of various factors, including the elastic modulus and thickness of the asphalt layer, the elastic modulus, and thicknesses of the cement concrete slab, as well as the dimensions of the cement concrete slab (length and width), foundation reaction modulus, and joint width, on the comprehensive stress at the bottom of the asphalt layer. Additionally, formulas were derived to calculate the temperature warping stress and load stress, and a formula was also provided for determining the equivalent modulus of the structure, taking into account the stress-absorbing layer. Subsequently, the proposed methodology was applied to the Weixu Expressway. The results suggest adopting a surface structure design scheme consisting of a 6 cm asphalt concrete + 2 cm stress absorption layer. This study found that, when the thickness of the stress-absorbing layer is less than 2 cm, the load stress is highly sensitive to changes in the thickness of this layer. Specifically, a 1 cm thick stress-absorbing layer reduces the maximum tensile stress at the bottom of the asphalt layer by approximately 69.7%, decreases the equivalent stress by about 34.1%, and lowers the maximum shear stress by around 30.9%. However, once the thickness exceeds 2 cm, the load stress remains relatively constant. Thus, it was advisable to utilize an optimal stress-absorbing layer thickness of 2 cm.

Keywords: composite pavement; design method; asphalt layer; cement concrete slab; comprehensive stress; tensile strength

check for updates

Academic Editor: Luís Picado Santos

Received: 2 January 2025
Revised: 26 January 2025
Accepted: 5 February 2025
Published: 7 February 2025

Citation: Fang, N.; Wang, X.; Chang, H.; Yu, K. Design Approach for Composite Pavement Structure Incorporating Reflective Crack Considerations. *Appl. Sci.* **2025**, *15*, 1691. https://doi.org/10.3390/app15041691

Copyright: © 2025 by the authors. Licensee MDPI, Basel, Switzerland. This article is an open access article distributed under the terms and conditions of the Creative Commons Attribution (CC BY) license (https://creativecommons.org/licenses/by/4.0/).

1. Introduction

With the continuous rise in modern traffic volume, there has been a gradual increase in the utilization of composite pavement structures [1,2]. Distinguished from traditional semi-rigid pavement structures, composite pavement employs a thinner asphalt layer and a thicker cement concrete layer as its composite surface, offering the advantages of reduced asphalt consumption and addressing the shortcomings of rigid pavements, such as joints

that can affect driving comfort and stability [3,4]. Nevertheless, the substantial disparity in material modulus between the rigid and flexible pavement layers gives rise to the challenge of disparate pavement deformation. Hence, the determination of the appropriate asphalt layer thickness holds a major significance in pavement structure design [5,6].

Currently, the design methods employed for composite pavement structures encompass several approaches. The American Asphalt Association's AI deflection method [7] primarily emphasizes the control of average deflection and deflection discrepancies at slab edges near joints or cracks. It prescribes that the deflection difference between the two slab edges at joints or cracks should not exceed 0.05 mm, and the average deflection value of these edges should remain below 0.36 mm. Furthermore, it recommends a minimum thickness of 10 cm for the asphalt surface layer. In situations where there are substantial variations in the temperature gradient, particularly when the maximum and minimum temperature differences exceed the daily average recorded over the past 30 years, a minimum asphalt overlay layer thickness of 20 cm is advised. However, it is important to note that this method relies on empirical determinations of asphalt layer thickness and lacks a scientific calculation foundation. The AASHTO (American Association of State Highway and Transportation Officials) method [8] employs the concept of equivalent thickness to determine the appropriate thickness of asphalt layers, incorporating comprehensive factor corrections to enhance flexibility and facilitate widespread utilization. Consequently, this method achieves better alignment with real-world projects. However, it overlooks control parameters pertaining to cracks in cement concrete pavement following the addition of the asphalt surface layer. This oversight implies that the cement concrete pavement stabilizes and remains undamaged after the asphalt surface layer is applied, which does not align with actual conditions. The COE (Corps of Engineers) method, developed by the US Army Corps of Engineers [9,10], offers empirical formulas for calculating asphalt layer thickness through a combination of theoretical analysis and experimentation. The effective thickness method [7] is predicated on the notion that the overlay layer thickness should encompass the requirements of both the new road surface and the effective thickness of the existing road surface. Nonetheless, the formulas proposed by these methods exhibit relative simplicity and consider a limited number of factors. Additional design methods, such as the static model analysis method developed by Austin Research Engineers [11], the asphalt overlay design method based on fracture mechanics [12], and the analysis system implemented by the University of California, Berkeley [13], rely on foreign experiences to ascertain the appropriate thickness of the asphalt layer. In general, different countries have put forth composite pavement design methods tailored to their specific contexts, offering valuable insights for composite pavement design in China. However, it should be noted that these methods cannot be directly applied to the unique circumstances in China [14].

The design methodology for composite pavement structures outlined in China's "Design Specification for Highway Cement Concrete Pavements" [15] centers around the primary design criterion of preventing fractures in cement concrete slabs. The guiding principle of this approach is to ensure that, within the designated design period and under specified traffic and environmental conditions, the combined fatigue stress induced by vehicle loads (maximum stress) and temperature gradients (maximum stress) remains below the flexural tensile strength of concrete. Consequently, the flexural tensile strength of concrete serves as the crucial cracking indicator, and employing existing design formulas can effectively avert fatigue cracking at the bottom of the concrete slab. However, the design methodology exhibits a notable oversight concerning the joint between the bottom of the asphalt layer and the cement slab, which represents the most vulnerable stress location in composite pavement. Insufficient consideration and the absence of corresponding control indicators for this specific area have led to the prevalence of reflective cracks, constituting a

prevalent issue in composite pavement [16,17]. Presently, there is a lack of asphalt layer thickness design indicators and systems in China, leading to the predominant reliance on experiential determinations for asphalt layer thickness. Furthermore, insufficient attention has been given to the stress relaxation characteristics of asphalt layers in temperature stress analysis [4].

In conclusion, this article introduces the limit state equation for the initial cracking at the bottom joint of the asphalt layer in composite pavement. It proposes a design criterion for determining the appropriate thickness of the asphalt layer, which states that the comprehensive stress (comprising temperature stress and load stress) at the bottom of the asphalt layer should not exceed the tensile strength of the asphalt mixture. Additionally, a design methodology for determining the asphalt layer thickness in composite pavement is established. This methodology employs the bending tensile stress at the bottom of the slab as the control parameter for pavement structure design and utilizes the maximum tensile stress at the bottom joint of the asphalt layer as the verification criterion. As a result, the composite pavement structure design is governed by considerations of both the flexural tensile strength of the concrete cement slab bottom and the tensile strength of the asphalt mixture.

2. Enhancing the Design Methodology of Current Composite Pavement Structures

2.1. Design Methodology for Composite Pavement Structure

The occurrence of crack damage in composite pavement is depicted in Figure 1. The figure highlights two particularly critical stress locations within the composite pavement structure: the joint of the cement concrete slab corresponding to the bottom of the asphalt layer (referred to as "asphalt layer bottom position 1", representing the most unfavorable stress point for the asphalt layer bottom) and the bottom of the cement concrete slab. These stress points give rise to two distinct types of cracks. One type of crack, denoted as a reflection crack, arises due to the presence of joints in the cement board. At these joints, the bottom of the asphalt layer experiences substantial shear forces under both load and temperature conditions, resulting in the formation of reflection cracks. The other type of crack (denoted as a common crack) is attributed to the cracking of the bottom of the cement concrete slab, caused by the bending tensile stress exceeding the material's tensile strength. The design standard outlined in China's "Design Specification for Highway Cement Concrete Pavement" aims to prevent common cracks and is expressed through Equations (1) and (2). This design approach employs the bending tensile stress at the bottom of the concrete slab as the key parameter for assessing cracking and effectively addresses the occurrence of common cracks. However, it is noteworthy that the design formula lacks specific control measures for reflection cracks and fails to consider the stress conditions at position 1 of the asphalt layer bottom. Consequently, reflection cracks have emerged as a prevalent issue in composite pavement structures.

$$\gamma_r(\sigma_{pr} + \sigma_{tr}) \leq f_r \quad (1)$$

$$\gamma_r(\sigma_{pm} + \sigma_{tm}) \leq f_r \quad (2)$$

where γ_r depicts the reliability coefficient; σ_{pr} is the load fatigue stress of cement concrete slabs at unfavorable locations, MPa; σ_{tr} denotes the temperature fatigue stress of cement concrete slabs at unfavorable positions, MPa; σ_{pm} is the maximum load stress at the most unfavorable position of the cement concrete slab under the heaviest axle load, MPa; σ_{tm} represents the maximum temperature stress at the most unfavorable position of the cement

concrete slab at the maximum temperature gradient in the region, MPa; f_r is the standard value of flexural tensile strength of cement concrete, MPa.

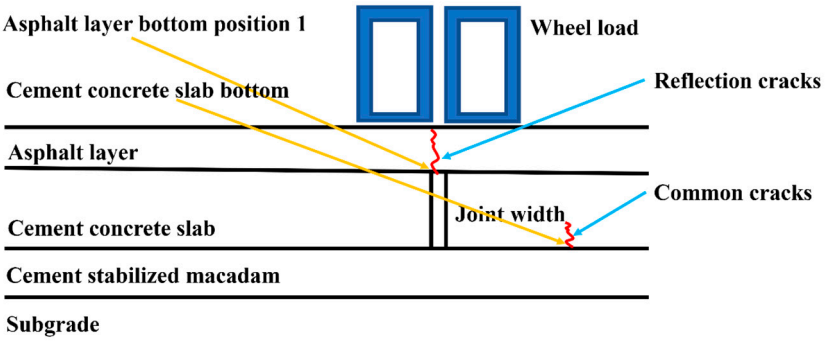


Figure 1. Main diseases of composite pavement.

This article enhances the current design approach for composite pavement structures by revising the design indicators. Specifically, the focus is on two key aspects [18–20]: (1) The prevention of fatigue cracking at the bottom of cement concrete slabs, which is governed by the bending and tensile strength of the cement concrete as stipulated in the specifications. The corresponding calculation formulas are presented in Equations (1) and (2). (2) The mitigation of cracking at the bottom of the asphalt layer, which is regulated by the bending and tensile strength of the asphalt mixture. The derivation process for this aspect is outlined as follows:

In the presence of both temperature fluctuations and traffic loads, the bottom of the composite pavement's asphalt layer is susceptible to crack formation when the comprehensive stress exceeds the tensile strength of the asphalt mixture. Hence, the stress condition at the bottom of the asphalt layer, where the comprehensive stress does not surpass the corresponding tensile strength of the asphalt mixture, is defined as the limit state of the asphalt layer. This limit state is quantified by Equations (3) and (4):

$$\sigma_{tr0} + \sigma_{ps0} \leq \sigma_R \tag{3}$$

$$\sigma_{tr0} = k_{1t}(\sigma_{t0} + \sigma_x\lceil T\rceil) \tag{4}$$

Through extensive road surface and loop tests, fatigue tests have shown that the conversion equation for σ_R and strength σ_s is as shown in Equations (5) and (6):

$$\sigma_R = \frac{\sigma_s}{K_s} \tag{5}$$

$$K_s = 0.09A_aN_e^{0.22}/A_c \tag{6}$$

where σ_{tr0} depicts the temperature stress at position 1 at the bottom of the asphalt layer, MPa; σ_{ps0} is the load stress at position 1 of the bottom of the asphalt layer, MPa; σ_R represents the tensile strength of asphalt mixture, MPa; k_{1t} is the temperature stress correction coefficient at position 1 of the asphalt layer bottom; σ_{t0} is the temperature warping stress at position 1 of the bottom of the asphalt layer, MPa; $\sigma_x\lceil T\rceil$ reflects the temperature shrinkage stress considering relaxation, MPa; σ_s is the splitting strength of asphalt concrete materials, MPa; K_s is the structural coefficient of tensile strength of asphalt concrete materials; A_a means the coefficient of the gradation type for asphalt concrete; A_c is the highway grade coefficient; N_e is the accumulated equivalent standard axle load traffic times of a lane within the design period.

Equation (3) can be further rewritten as follows:

$$\sigma_{ps0} \leq \frac{\sigma_s}{K_s} - k_{1t}(\sigma_{t0} + \sigma_x\lceil T\rceil) \tag{7}$$

where σ_s represents the experimentally measured splitting strength of the asphalt mixture, while the values for K_s, k_{1t} are based on the existing standard values. The calculation process for $\sigma_x\lceil T\rceil$ can be found in the author's paper "Study on asphalt layer of composite pavement temperature shrinkage stress considering stress relaxation" [4]. σ_{ps0} is obtained through fitting using the eccentric force formula in material mechanics, as presented in Equations (9) and (10).

$$\sigma_x\lceil T\rceil = \sum_{T_0}^{T_f} G(T_i, t_i)\left(c_2 - \frac{a_1\sqrt{a_1+a_2}\cdot c_3}{a_2}A^l + \frac{a_1\sqrt{a_1+a_2}\cdot c_4}{a_2}A^{-l} - a_a\Delta T_i\right) \tag{8}$$

$$\sigma_{t0} = \left(\frac{N_t}{A} + \frac{6M_t}{h_1^2}\right) = \left(\frac{N_t}{h_1} + \frac{6M_t}{h_1^2}\right) \tag{9}$$

$$\sigma_{ps0} = \left(\frac{N_p}{A} + \frac{6M_p}{h_1^2}\right) = \left(\frac{N_p}{h_1} + \frac{6M_p}{h_1^2}\right) \tag{10}$$

where N_t, N_p is the axial force of the joint center section, N; M_t, M_p is the bending moment of the joint center section, N × m; A is the cross-sectional area, m^2; h_1 is the cross-sectional height, m; $A = bh_1$ and $b = 1$m; for a, c, and l, please refer to reference [4].

2.2. Design Process of Composite Pavement Structure

The design process for a new composite pavement structure can be systematically conducted by following the outlined steps, as illustrated in Figure 2:

(1) Systematic analysis of collected traffic parameters: Thoroughly examine the gathered traffic data and calculate the cumulative number of actions for the design lane's standard load.
(2) Preliminary design of pavement structure: Determine the materials and thickness for each layer of the road surface. Additionally, establish measures to prevent reflection cracks, including the selection of appropriate materials, their locations, and the desired thickness.
(3) Calculation of bending tensile stress at the bottom of the slab: Refer to the relevant specifications to assess whether the load stress and temperature stress are within the permissible limits of concrete's flexural and tensile strength.
(4) Verification of maximum tensile stress at the bottom of the asphalt layer: Calculate the temperature stress of the asphalt layer, considering a combination of temperature warping stress and stress relaxation-induced temperature shrinkage stress. Also, evaluate the maximum load stress at the critical point of the asphalt layer structure. If the sum of these stresses is below or near the allowable tensile stress at the bottom of the asphalt layer, the initially selected thickness can be considered as the calculated thickness for the asphalt layer.
(5) If it is not possible to satisfy both steps (3) and (4) simultaneously, it is necessary to reevaluate and adjust the thickness of the cement board and asphalt layer. Repeat the above steps until all the requirements are met.

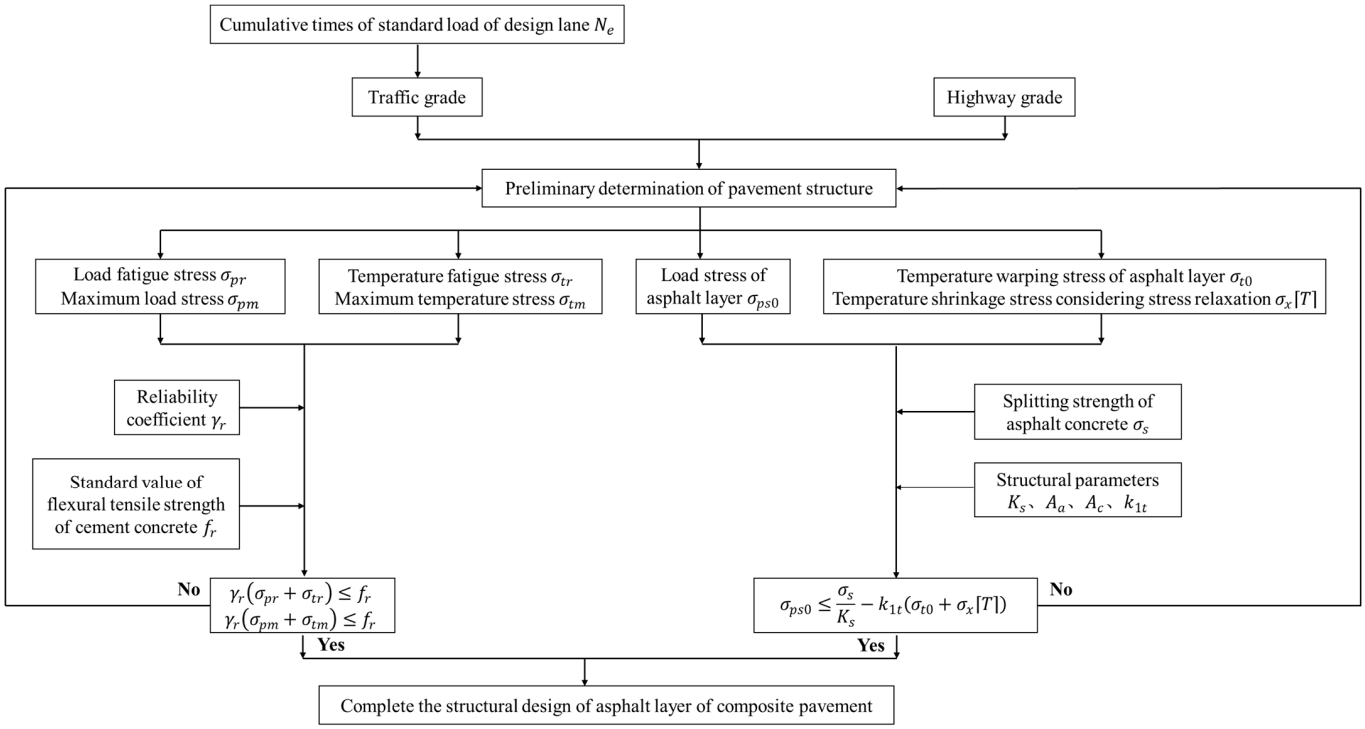


Figure 2. Design flow chart of composite pavement structure.

During the milling and paving process of the composite pavement, the thickness design of the asphalt layer can be adjusted based on the actual engineering conditions, while still adhering to the principles depicted in Figure 2.

3. Derivation of Calculation Formula for Temperature Warping Stress

3.1. Calculation Model for Temperature Warping Stress

To analyze the impact of the board warping phenomenon on the bottom position of the asphalt layer, the finite element method was employed in this study. This approach facilitates the consideration of the foundation reaction and the self-weight constraint of the board on warping stress [21,22]. When developing the temperature warping stress model, the following assumptions were made:

(1) Each structural layer of the road surface was a uniformly distributed and isotropic elastic body;
(2) Assuming that the temperature within the pavement structure remains constant laterally, heat transfer occurs only in the vertical (depth) direction of the pavement;
(3) The structural layers of the road surface were in close contact and exhibited continuous heat transfer.

The finite element model is employed to calculate the thermal stresses, and the specific implementation steps are as follows: (1) Determine the material properties of each layer in the pavement structure. (2) Assign various parameters for the materials, as shown in Table 1. (3) Apply the material properties to the model and then discretize the model by meshing. (4) Apply temperature loads according to the temperature gradient. The positive temperature gradient is set up, meaning the surface temperature of the slab is higher than the bottom, causing the edges of the slab to curl upwards, resulting in tensile stress at the bottom of the slab. (5) Solve the model and extract the thermal warping stresses at position 1 on the bottom of the asphalt layer and the interlayer shear stresses.

Table 1. Benchmark model parameters.

	Length (m)	Thickness (m)	Elastic Modulus (MPa)	Poisson's Ratio	Density (kg/m^3)	Thermal Conductivity (J/m·h·°C)	Specific Heat (J/kg·°C)	Coefficient of Thermal Expansion (/°C)
Asphalt layer	8.01	0.06	2000	0.20	2400	4680	924.9	0.00002
Cement concrete slab	4 + 2	0.28	30,000	0.15	2400	5616	911.7	0.00001
Cement stabilized macadam	8.01	0.18	2600	0.15	2350	5616	911.7	0.00001
Joint width					0.01			
Interlayer state (Asphalt layer + cement concrete layer)	The interlayer is smooth							
Interlayer state (Cement concrete layer + base course)	The interlayer is completely continuous							

Furthermore, relevant research [23] indicated that the distribution of cross-sectional stress along the thickness in both three-dimensional and planar models showed good consistency under temperature gradients. Any variations between the two models were minimal and mainly existed in regions with high stress concentrations. Considering the need for computational efficiency, this study adopted a planar model.

Different temperature gradients cause thermal contraction deformation in the concrete slab, which alters the stress at position 1 on the bottom of the asphalt layer. Given that this position is the most critical stress point within the pavement structure, The stress was calculated at position 1 of the asphalt layer bottom under six temperature gradients: −50 °C/m, −40 °C/m, −30 °C/m, 30 °C/m, 40 °C/m, and 50 °C/m. The calculation results are shown in Figure 3.

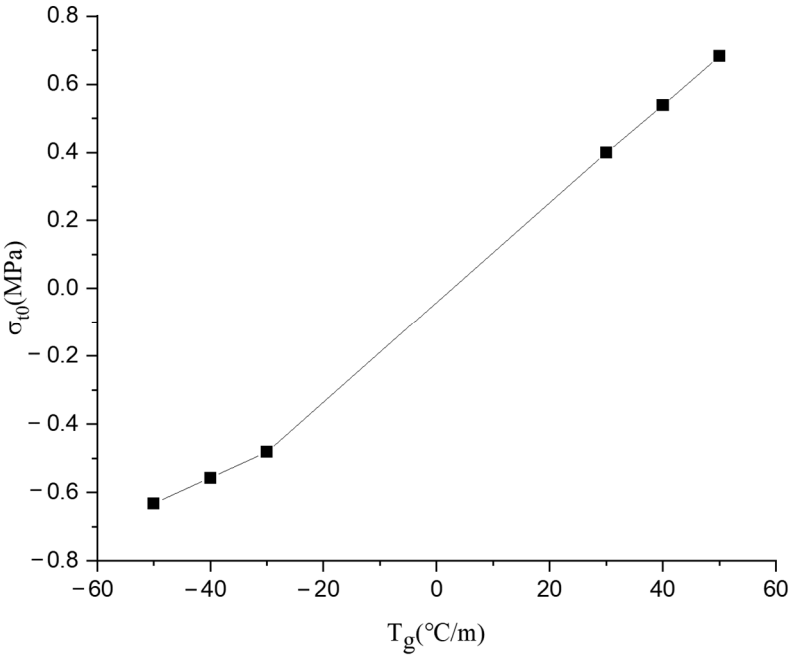


Figure 3. Different temperature gradients respond to warping stress values.

Based on Figure 3, it can be observed that, as the temperature gradient increased, the warping stress also increased. This was because the temperature difference across the plate increased with a higher temperature gradient, resulting in elevated temperature warping stress. For the concrete slab, under the same temperature gradient, the effect of a negative temperature gradient on its temperature warping stress was slightly smaller compared to a positive temperature gradient. Previous research [3] has indicated that positive temperature gradients in pavement structures were generally much larger than negative temperature gradients. Therefore, the subsequent analysis focused on the influence of various structural parameters on temperature stress when considering a temperature gradient of 50 °C/m [23].

3.2. The Effect of Structural Parameters on Temperature Warping Stress

In previous research [23], several factors were identified as the main influencers of temperature warping stress in asphalt layers, including the elastic modulus of the asphalt layer (E_1), the thickness of the asphalt layer (h_1), the elastic modulus of the cement concrete slab (E_2), the thickness of the cement concrete slab (h_2), the length of the cement concrete slab (L), and the foundation reaction modulus (k). The stress indicators analyzed were the temperature warping stress and interlayer shear stress at position 1, which is the bottom of the asphalt layer under a temperature gradient.

(1) The influence of E_1

As depicted in Figure 4, an increase in E_1 led to a gradual increase in both temperature stress and interlayer shear stress. Specifically, for each increment in modulus from 500 MPa, the temperature warping stress approximately doubled. However, the increase in interlayer shear stress was not significant. When E_1 reached 4000 MPa, the shear stress was only 0.00651 MPa, and when E_1 increased to 10,000 MPa, the shear stress was 0.0124 MPa.

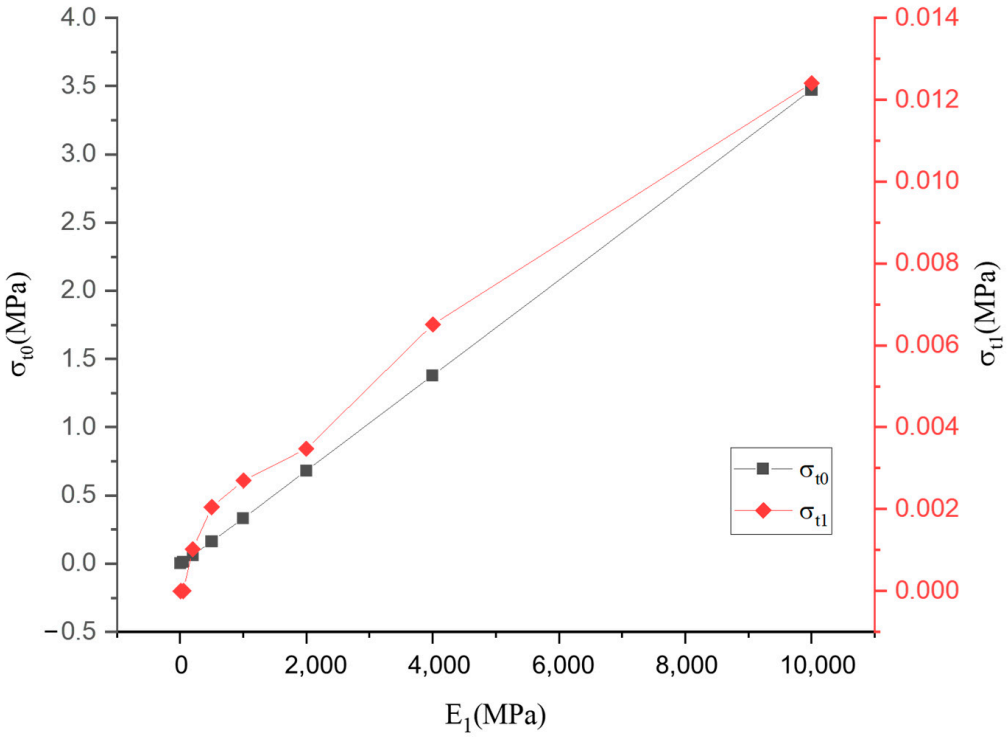


Figure 4. Temperature stress at different E_1 values.

(2) The influence of h_1

Figure 5 illustrates that, with an increase in h_1, both the temperature warping stress and interlayer shear stress exhibited a gradual decrease. Specifically, for every 4 cm increment in h_1, the reduction in warping stress under a temperature gradient ranged from approximately 1.3% to 7.8%. On the other hand, the decrease in interlayer shear stress was minimal, with the minimum interlayer shear stress recorded at 0.00299 MPa and the maximum interlayer shear stress at 0.00358 MPa.

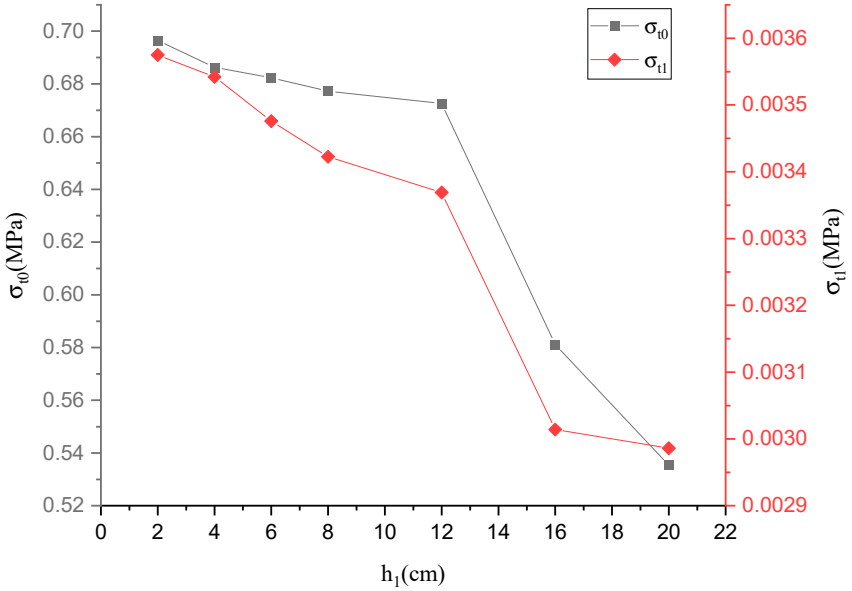


Figure 5. Temperature stress at different h_1 values.

(3) The influence of E_2

In Figure 6, it is evident that the temperature warping stress and interlayer shear stress gradually increased with an increase in E_2. Specifically, under the influence of a temperature gradient, for every 500 MPa increased in E_2, the warping stress exhibited an approximate 3% increment. On the other hand, the increase in interlayer shear stress was minimal, with the minimum interlayer shear stress recorded at 0.00233 MPa and the maximum interlayer shear stress at 0.00412 MPa.

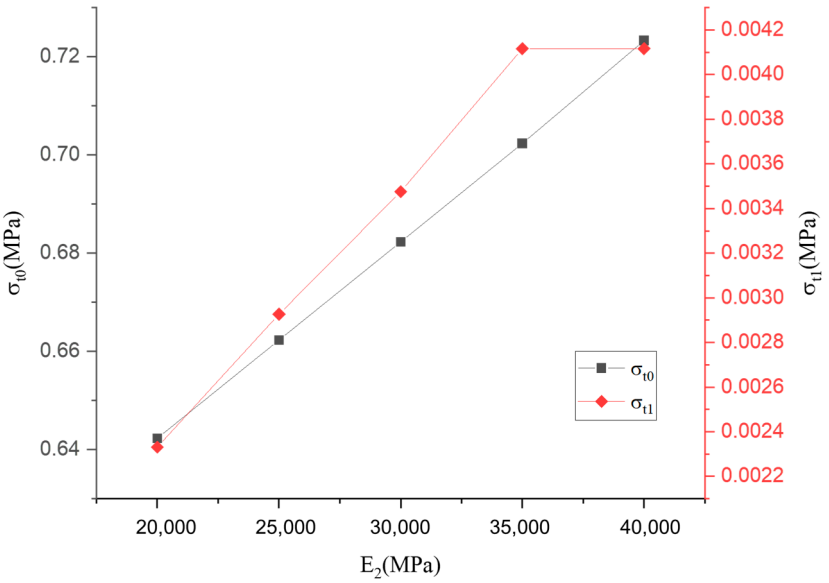


Figure 6. Temperature stress at different E_2 values.

(4) The influence of h_2

According to the findings presented in Figure 7, it is observed that an increase in h_2 corresponded to a gradual increase in both temperature warping stress and interlayer shear stress. When subjected to a temperature gradient, each 0.02 m increment in h_2 led to an approximate increase of 1.7–6.1% in the warping stress. However, the impact on the interlayer shear stress was negligible, with the minimum value recorded at 0.00248 MPa and the maximum at 0.00478 MPa.

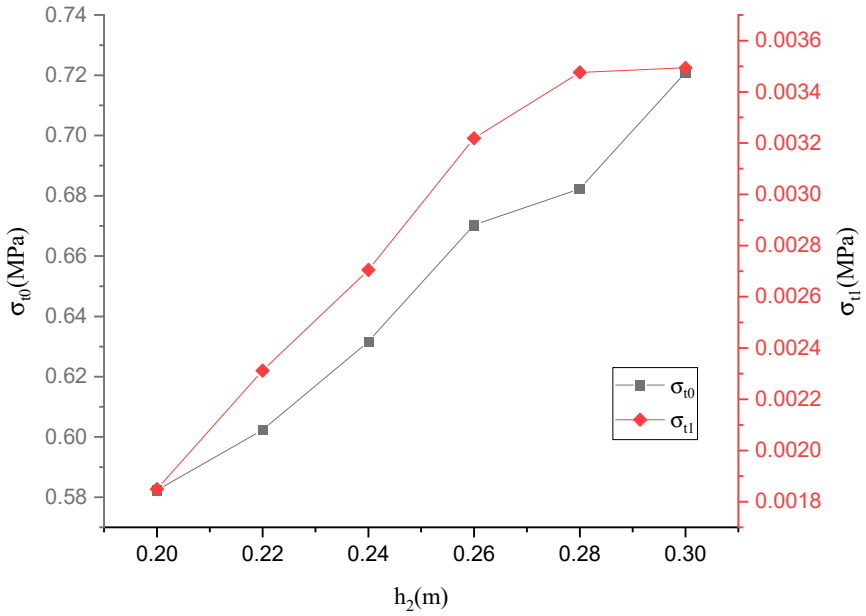


Figure 7. Temperature stress at different h_2 values.

(5) The influence of L

As shown in Figure 8, as L increased, the temperature warping stress was found to gradually decrease. Under the effect of a temperature gradient, L increased from 3.8 m to 5.2 m, and the decrease in the temperature warping stress was noted to be about 1.4%. The interlayer shear stress remained basically unchanged, always at 0.00348 MPa.

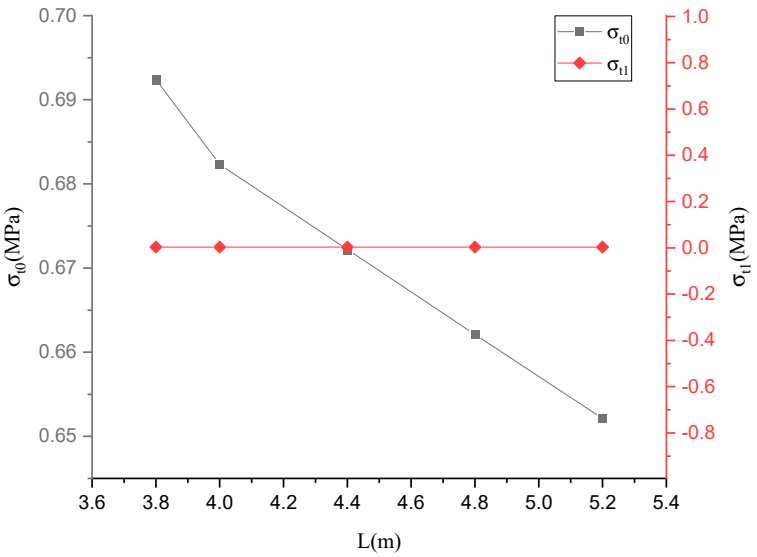


Figure 8. Temperature stress at different L values.

(6) The influence of k

As shown in Figure 9, an increment in k caused a gradual decrease in the temperature warping stress. Under the effect of a temperature gradient, the decrease in the temperature warping stress was about 10–15% for every doubling of k. The decrease in the interlayer shear stress was negligible, with a minimum interlayer shear stress of 0.00335 MPa and a maximum interlayer shear stress of 0.00348 MPa.

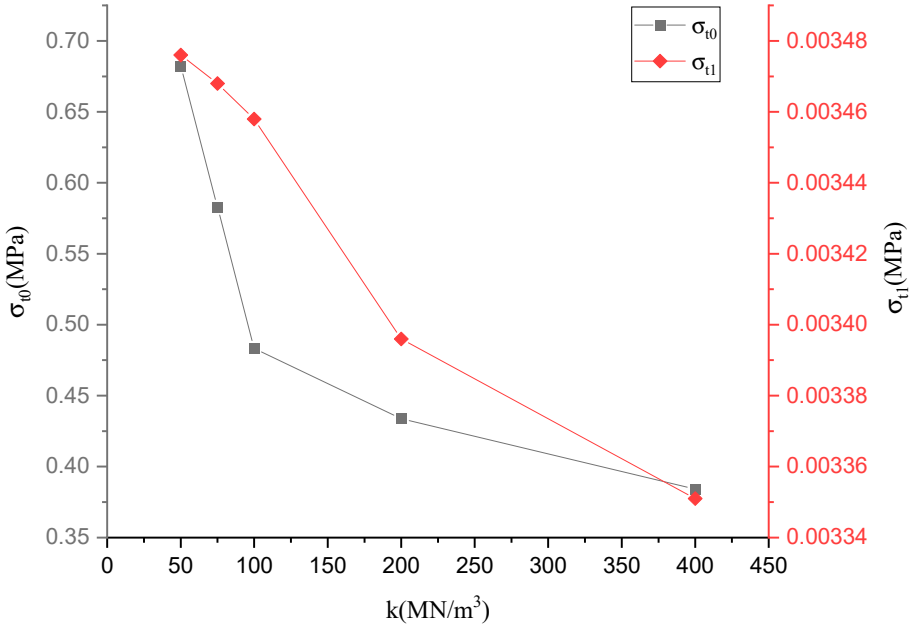


Figure 9. Temperature stress at different k values.

3.3. Formula for Calculating Temperature Warping Stress

In Equation (9), N_t is as shown in Equations (11) and (12):

$$N_t = \alpha_c E_1 T_g h_1 h_2 \varphi_N \tag{11}$$

$$\varphi_N = Ag(E_1/E_2)g(h_1)g(h_2)g(k) \tag{12}$$

where α_c depicts the shrinkage coefficient, taken as 0.00001; T_g is the temperature gradient, taken as 50 °C/m; φ_N represents the correction factor for the axial force of the section; $A, g(E_1/E_2), g(h_1), g(h_2), g(k)$ is the fitted parameter or formula.

In Equation (9), M_t is as shown in Equations (13) and (14):

$$M_t = \alpha_c E_1 T_g {h_1}^2 h_2 \varphi_M \tag{13}$$

$$\varphi_M = Bf(E_1/E_2)f(h_1)f(h_2)f(k) \tag{14}$$

where φ_M is the section bending moment correction factor; $B, f(E_1/E_2), f(h_1), f(h_2), f(k)$ is the fitted parameter or formula.

Using the Levenberg–Marquardt algorithm, a program was written to fit a total of 22 parameters after 185 iterations. The correlation coefficient between the simulated and measured values was determined to be 0.99013, indicating a strong correlation. Furthermore, the root mean square error was calculated to be 0.08838, indicating a small deviation between the fitted values and the actual values. The fitted value for σ_{t0} can be found in Equations (15)–(19).

$$\sigma_{t0} = \left(\frac{N_t}{h_1} + \frac{6M_t}{h_1^2}\right) \tag{15}$$

$$\begin{aligned} N_t &= \alpha_c E_1 T_g h_1 h_2 Ag\left(\tfrac{E_1}{E_2}\right)g(h_1)g(h_2)g(k) \\ &= 0.00001 \times 50 E_1 h_1 h_2 Ag\left(\tfrac{E_1}{E_2}\right)g(h_1)g(h_2)g(k) \end{aligned} \tag{16}$$

$$\begin{cases} A = 0.8119 \\ g(E_1/E_2) = 0.9344 + 0.8849e^{0.9449(E_1/E_2)} \\ g(h_1) = 0.9162 + 0.9037e^{0.9874h_1} \\ g(h_2) = 0.8119{h_2}^{1.1796} \\ g(k) = 0.8119k^{-0.0726} \end{cases} \quad (17)$$

where A is a constant parameter; $g(E_1/E_2)$ represents the influence of the ratio between the asphalt layer modulus and the cement slab modulus on N_t; $g(h_1)$ represents the influence of the thickness of the asphalt layer on N_t; $g(h_2)$ represents the influence of the thickness of the cement slab on N_t; $g(k)$ represents the influence of the subgrade reaction modulus on N_t.

$$\begin{aligned} M_t &= \alpha_c E_1 T_g {h_1}^2 h_2 B f(E_1/E_2) f(h_1) f(h_2) f(k) \\ &= 0.00001 \times 50 E_1 {h_1}^2 h_2 B f(E_1/E_2) f(h_1) f(h_2) f(k) \end{aligned} \quad (18)$$

$$\begin{cases} B = 0.8887 \\ f(E_1/E_2) = 1.0147 + 0.8679e^{0.8304(E_1/E_2)} \\ f(h_1) = 0.9589 + 0.9291e^{0.9691h_1} \\ f(h_2) = 0.8887{h_2}^{0.9844} \\ f(k) = 0.8887k^{-0.2117} \end{cases} \quad (19)$$

where B is a constant parameter; $f(E_1/E_2)$ represents the influence of the ratio between the asphalt layer modulus and the cement slab modulus on M_t; $f(h_1)$ represents the influence of the thickness of the asphalt layer on M_t; $f(h_2)$ represents the influence of the thickness of the cement slab on M_t; $f(k)$ represents the influence of the subgrade reaction modulus on M_t.

4. Derivation of Calculation Formula for Load Stress

4.1. Calculation Model for Load Stress

A three-dimensional model is employed to simulate the pavement structure in this study, wherein the load transfer between joints is represented by spring stiffness. The three-dimensional finite element model is set up with ABAQUS, and the C3D8R element is used. The pavement structure layer material is assumed to be isotropic; X, Y, and Z are the driving direction, depth direction, and cross-section direction, respectively. The parameters of the benchmark model are given in Table 2. In what follows, when the different parameters of Table 2 are changed, the corresponding factor can be changed on the basis of the benchmark model. The methodology for simulating the springs and calculating the stiffness can be found in the author's publication titled "Load Transfer Efficiency Analysis and Void Evaluation of Composite Pavement Cement Concrete Laboratory" [24]. The schematic diagram of joint stiffness and cement concrete slab nodes are shown in Table 3 and Figure 10, respectively.

Table 2. Benchmark model parameters (load).

	Length (m)	Width (m)	Thickness (m)	Elastic Modulus (MPa)	Poisson's Ratio
Asphalt layer	8.01	3	0.06	2000	0.20
Cement concrete slab	4 + 2	3	0.28	30,000	0.15
Cement stabilized macadam	8.01	3	0.18	2600	0.15
Joint width	0.01				
Interlayer state (Asphalt layer + cement concrete layer)	The interlayer is smooth				
Interlayer state (Cement concrete layer + base course)	The interlayer is completely continuous				

Table 3. Joint stiffness at different points of the slab.

Point	Spring Stiffness at Cement Concrete Slab Corner	Spring Stiffness in Cement Concrete Slab Center	Spring Stiffness at Cement Concrete SLAB Edge
Stiffness ($N \times m^{-1}$)	1.5×10^7	3.0×10^7	6.0×10^7

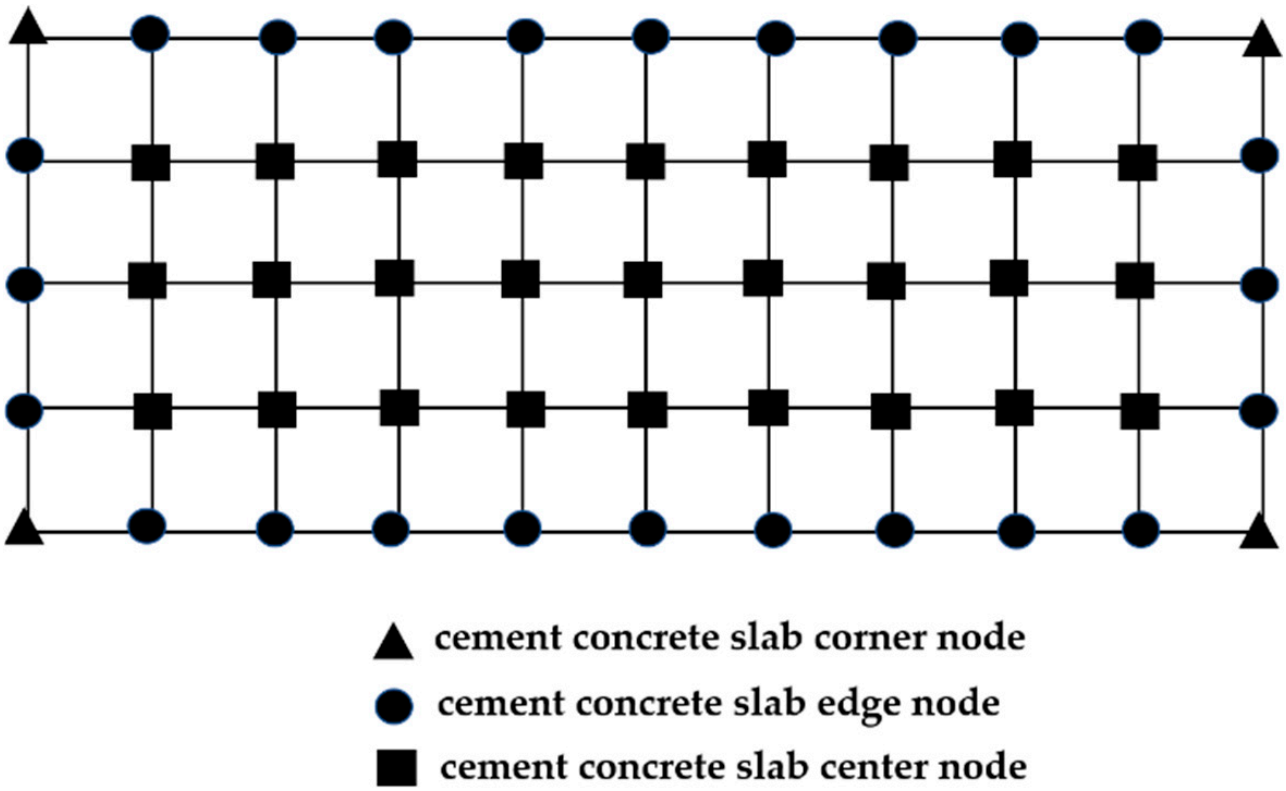


Figure 10. Schematic diagram of nodes of cement concrete slab.

4.2. The Effect of Structural Parameters on Load Stress

In previous studies [24], it has been demonstrated that the primary factors influencing load stress in asphalt layers include the elastic modulus E_1, the asphalt layer thickness h_1, the cement concrete slab elastic modulus E_2, the cement concrete slab thickness h_2, the length and width of cement concrete slab L * B, the foundation reaction modulus k, and the joint width δ. The analysis stress index encompasses the bending tensile stresses σ_x and σ_z, at position 1 at the bottom of the asphalt layer, as well as the interlayer tensile stress σ_y.

(1) The influence of E_1

As shown in Figure 11, increasing the elastic modulus E_1 leads to a gradual rise in the values of σ_x, σ_y, and σ_z. Specifically, when E_1 increases from 500 MPa, each doubling of the modulus results in a 20–40% increase in σ_x, a 6–8% increase in σ_z, and a 7% increase in σ_y. Previous studies [25,26] have identified a direct correlation between a decrease in temperature and an increase in E_1, with higher moduli contributing to greater load stresses. Additionally, cooling adversely affects the distribution of both temperature and load stresses in composite pavements.

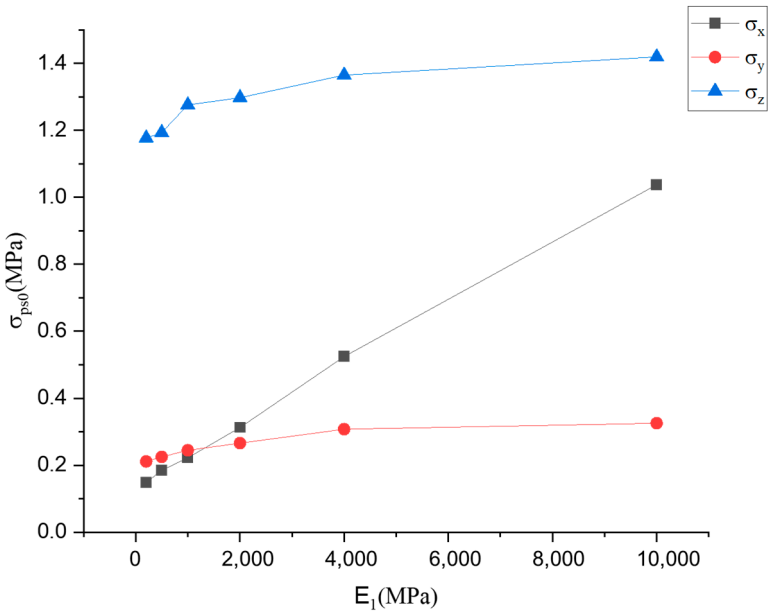


Figure 11. Load stress at different E_1 values.

(2) The influence of h_1

As depicted in Figure 12, increasing the thickness h_1 of the asphalt layer results in a decrease in the values of σ_x, σ_z, and σ_y. When h_1 increases to 12 cm, the reductions in σ_z and σ_y become more pronounced, reaching 50% and 30%, respectively.

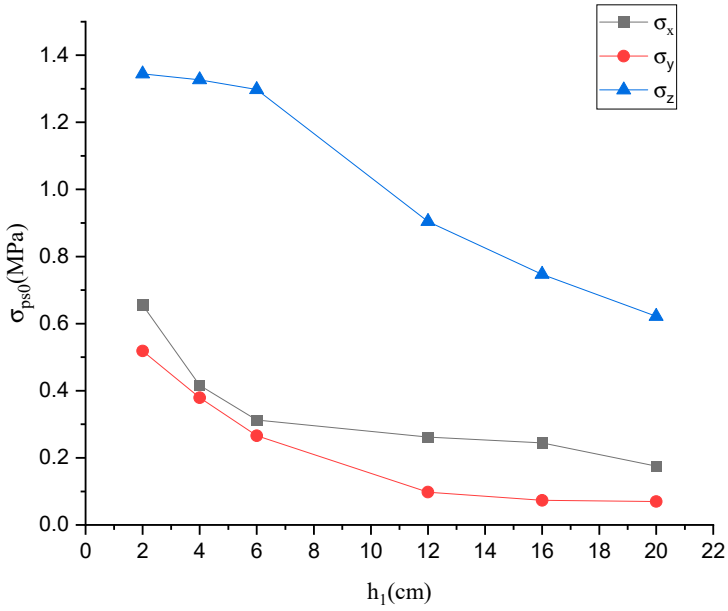


Figure 12. Load stress at different h_1 values.

(3) The influence of E_2

As shown in Figure 13, an increase in E_2 leads to a gradual decrease in σ_x and σ_z, while σ_y increases. For every 5000 MPa increase in the modulus of the cement board, σ_x increases by 6–10%, σ_z increases by 4–6%, and σ_y decreases by approximately 1%.

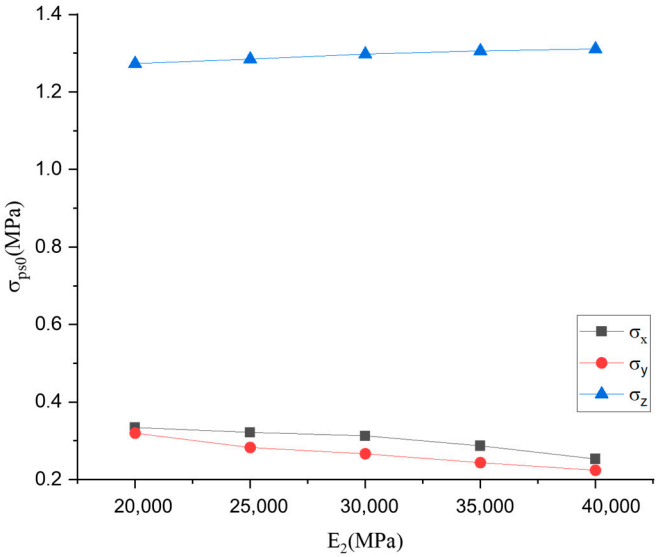


Figure 13. Load stress at different E_2 values.

(4) The influence of h_2

Figure 14 demonstrates that, as the thickness h_2 of the cement concrete slab increases, there is a gradual decrease in the values of σ_x, σ_z, and σ_y, albeit not significantly. Specifically, for every 2 cm increase in h_2, σ_x decreases by approximately 6–10%, σ_z decreases by 3–6%, and σ_y decreases by 1–4%.

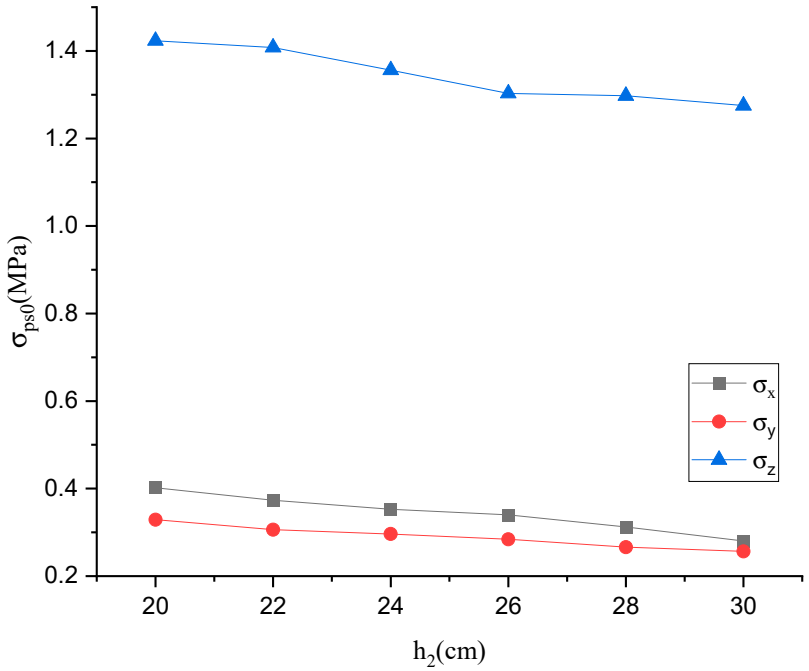


Figure 14. Load stress at different h_2 values.

(5) The influence of L * B

As shown in Figure 15, increasing L * B results in a gradual decrease in σ_x, σ_z, and σ_y. Specifically, σ_x decreases by 15–20%, σ_z decreases by 2–7%, and σ_y decreases by 1.5–1.9%. Smaller dimensions of L * B in cement concrete slabs reduce load fatigue stress. For instance, the Weixu Expressway employs cement concrete slabs with dimensions of 4.0 m in length and 3.0 m in width, a design that minimizes load stress and prolongs the service life of the composite pavement by allowing vehicles to pass over cracks more effectively.

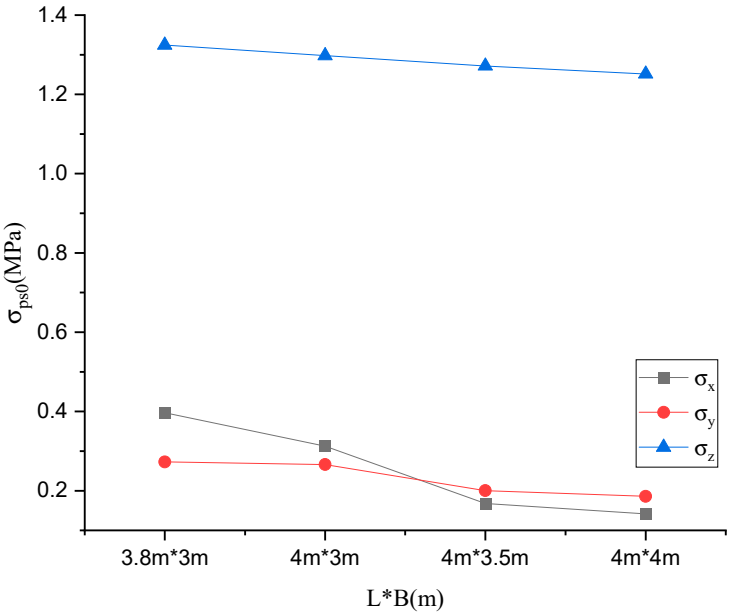


Figure 15. Load stress at different $L * B$ values.

(6) The influence of k

As shown in Figure 16, an increase in k leads to a gradual decrease in σ_x, σ_z, and σ_y. Specifically, σ_x decreases by 6–18%, σ_z decreases by 8–9%, and σ_y decreases by 4–8%. Therefore, a higher value of k is beneficial for reducing the load stress experienced by the asphalt layer.

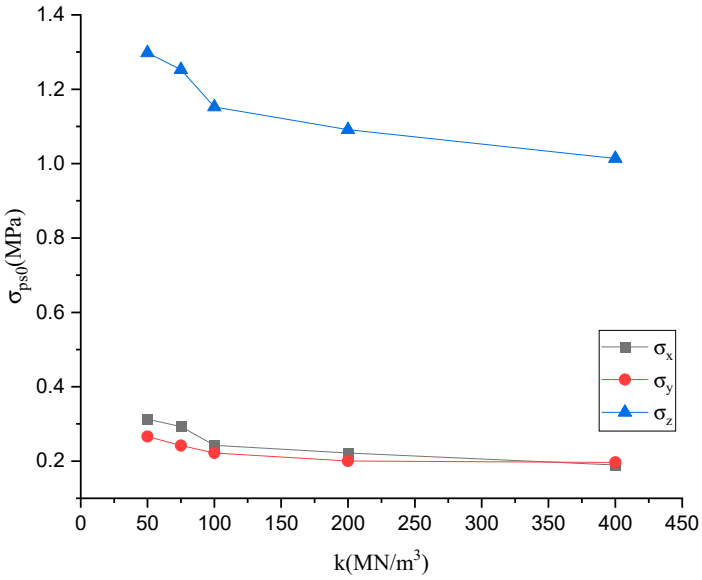


Figure 16. Load stress at different k values.

(7) The influence of δ

Figure 17 illustrates that, as δ increases, σ_x and σ_z increase gradually, while σ_y decreases. For every 5 mm increment in δ, σ_x increases by 20%, σ_z increases by 11%, and σ_y decreases by 10%. A larger joint width helps reduce interlayer tensile stress, although it may negatively affect the bending tensile stress at the bottom of the asphalt layer.

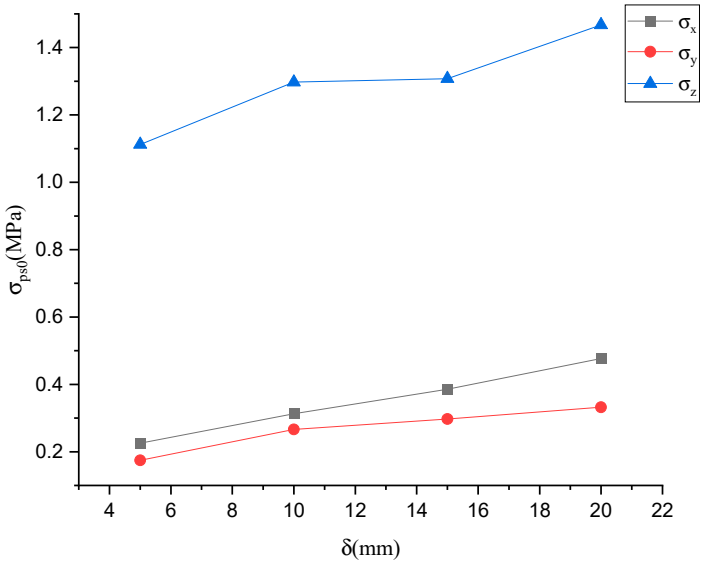


Figure 17. Load stress at different δ values.

4.3. Formula for Calculating Load Stress

In Equation (10), N_p is as shown in Equations (20) and (21):

$$N_p = Ph_1\varphi_{PN} \tag{20}$$

$$\varphi_{PN} = Ag(E_1/E_2)g(h_1)g(h_2)g(k)g(\delta) \tag{21}$$

where P is the standard axile load, taken as 100 kN; φ_{PN} is the correction factor for the axial force of the section; $A, g(E_1/E_2), g(h_1), g(h_2), g(k), g(\delta)$ is the fitted parameter or formula.

In Equation (10), M_p is as shown in Equations (22) and (23):

$$M_p = Ph_1{}^2\varphi_{PM} \tag{22}$$

$$\varphi_{PM} = Bf(E_1/E_2)f(h_1)f(h_2)f(k)f(\delta) \tag{23}$$

where φ_{PM} is the section bending moment correction factor; $B, f(E_1/E_2), f(h_1), f(h_2), f(k), g(\delta)$ is the fitted parameter or formula.

σ_{t0} uses the same calculation method, and a program was written to fit a total of 26 parameters after 188 iterations. With a correlation coefficient of 0.86626 and a root mean square error of 0.0816, the program's ability to meet engineering calculation requirements in most cases is confirmed. Equations (24)–(28) provide the expression for σ_{ps0}.

$$\sigma_{ps0} = \left(\frac{N_p}{h_1} + \frac{6M_p}{h_1^2}\right) \tag{24}$$

$$N_p = Ph_1Ag(E_1/E_2)g(h_1)g(h_2)g(k)g(\delta) \tag{25}$$

$$\begin{cases} A = 0.1141 \\ g(E_1/E_2) = 0.1056 + 0.1075e^{0.1021(E_1/E_2)} \\ g(h_1) = 0.1067 + 0.1063e^{0.0995h_1} \\ g(h_2) = 0.1114 + 0.1020h_2 \\ g(k) = 0.1141k^{0.0997} \\ g(\delta) = 0.1003\delta + 0.1137 \end{cases} \tag{26}$$

where A is a constant parameter; $g(E_1/E_2)$ represents the influence of the ratio between the asphalt layer modulus and the cement slab modulus on N_p; $g(h_1)$ represents the influence

of the thickness of the asphalt layer on N_p; $g(h_2)$ represents the influence of the thickness of the cement slab on N_p; $g(k)$ represents the influence of the subgrade reaction modulus on N_p; $g(\delta)$ represents the influence of the joint width on N_p.

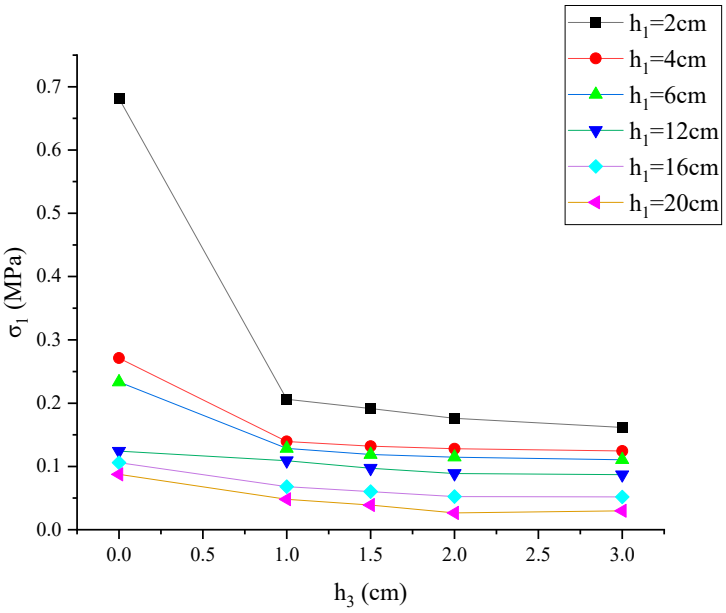
$$M_p = P{h_1}^2 B f(E_1/E_2) f(h_1) f(h_2) f(k) f(\delta) \tag{27}$$

$$\begin{cases} B = 0.4456 \\ f(E_1/E_2) = -0.3264 + 0.3437e^{0.6974(E_1/E_2)} \\ f(h_1) = 0.3310 + 0.3057e^{0.0201h_1} \\ f(h_2) = 0.4456 + {h_2}^{-0.1213} \\ f(k) = 0.4456k^{-0.1555} \\ f(\delta) = 0.1060\delta + 0.4439 \end{cases} \tag{28}$$

where B is a constant parameter; $f(E_1/E_2)$ represents the influence of the ratio between the asphalt layer modulus and the cement slab modulus on M_p; $f(h_1)$ represents the influence of the thickness of the asphalt layer on M_p; $f(h_2)$ represents the influence of the thickness of the cement slab on M_p; $f(k)$ represents the influence of the subgrade reaction modulus on M_p; $g(\delta)$ represents the influence of the joint width on M_p.

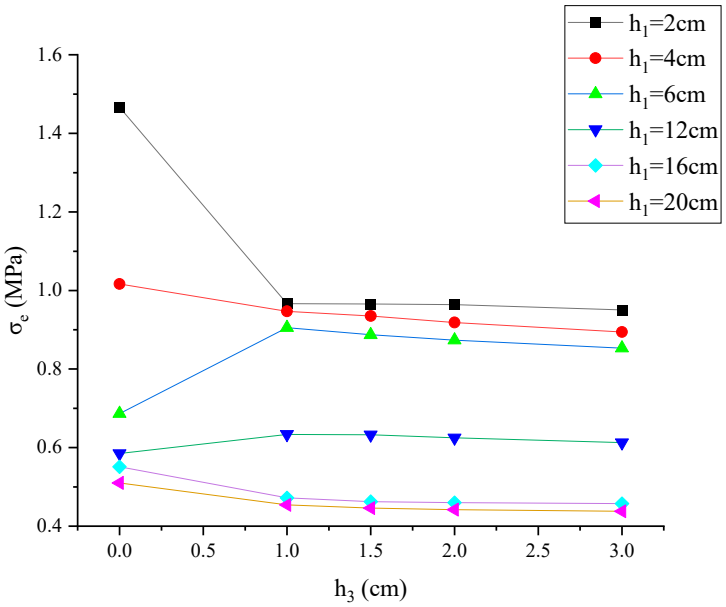
4.4. Load Stress Analysis of Composite Pavement Considering Stress Absorption Layer

While it has been acknowledged in engineering that the incorporation of stress-absorbing layers can enhance the crack resistance of road surfaces [27,28], quantitatively characterizing this structural performance remains challenging. In this study, a three-dimensional finite element model is utilized, incorporating a stress-absorbing layer modulus of 600 MPa. The analysis focuses on varying h_1 and the thickness of the stress-absorbing layer h_3. Subsequently, the maximum tensile stress σ_1, equivalent stress σ_e, and maximum shear stress τ_{max} of the asphalt layer when h_1 = 2 cm, 4 cm, 6 cm, 12 cm, 16 cm, and 20 cm and h_3 = 0 cm, 1 cm, 1.5 cm, 2 cm, and 3 cm are calculated. The calculation results are shown in Figure 18.

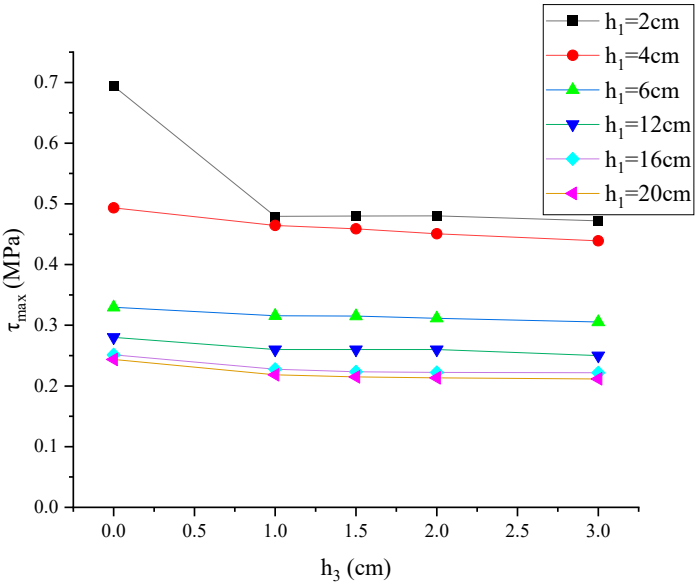


(**a**) $\sigma_1$for different h_1 and h_3 values

Figure 18. *Cont.*



(**b**) σ_e for different h_1 and h_3 values



(**c**) τ_{max} for different h_1 and h_3 values

Figure 18. σ_1, σ_e, and τ_{max} for different h_1 and h_3 values.

Based on the findings depicted in Figure 18, the following observations can be made:

(1) Setting a stress-absorbing layer can significantly reduce load stress. Setting a 1 cm stress-absorbing layer reduces σ_1 by 69.7% and σ_e by 34.1% compared to the absence of a stress-absorbing layer, and τ_{max} reduced by 30.9%.

(2) Increasing h_3 can effectively mitigate load stress. When h_3 is less than 2 cm, the load stress decreases as thickness increases. However, once h_3 is greater than 2 cm, the load stress remains relatively unchanged.

(3) The greater the value of h_1, the smaller the impact of the increase in h_3 on load stress.

Hence, the establishment of an appropriate thickness stress-absorbing layer is considered an effective approach for delaying the occurrence of reflection cracks. The research by Wu [29] proposed that the stress-absorbing layer cannot be treated as a single structural

layer and can be considered as a whole with the asphalt layer. The equivalent equation is given as follows:

$$E_c = \left(\frac{E_1^{1/3} h_1 + E_3^{1/3} h_3}{h_1 + h_3} \right)^3 \quad (29)$$

where E_c is the equivalent elastic modulus.

The aforementioned equation demonstrates that the equivalent elastic modulus is comparatively lower than that of the asphalt layer, while the tensile strength is higher. This disparity elucidates the ability of the stress-absorbing layer to impede or postpone cracking; however, it also underscores the limitation of excessive thickness in such a layer. As a result, while calculating the pavement structure when thinking about adding a stress-absorbing layer, the equivalent modulus conversion can be completed first and then the pavement structure design.

5. Engineering Examples

5.1. Engineering Status Survey

This study encompasses the design of composite pavement structure thickness for the Weixu Expressway in Henan Province, aiming to validate the efficacy of this approach. Following over a decade of usage, the surface layer of Weixu Expressway has exhibited various deteriorations, prompting the Highway Management Group to undertake extensive repairs on specific sections of the expressway. In order to ascertain the strength of the preexisting cement concrete slab, an on-site drilling operation yielded a cement concrete specimen measuring 150 mm in diameter and 28 cm in height. Figure 19 illustrates the condition of the specimen, while Table 4 presents the corresponding test outcomes.



Figure 19. Cement concrete specimens.

Table 4. Compressive strength and flexural tensile strength of cement concrete specimens.

Number	Maximum Tensile Force (kN)	Compressive Strength (MPa)	Flexural Tensile Strength (MPa)
P-1	526.9	36.81	4.5
P-2	500.4	34.96	4.5
P-3	366.6	25.61	4.0
P-4	538.9	37.65	4.5
P-5	529.1	36.97	4.5
P-6	400.5	27.98	4.0

During the design phase of the Weixu Expressway in 2008, the specified compressive strength of the cement concrete was 6.0 MPa, while the flexural tensile strength was 52.5 MPa. However, based on the obtained core sample, the compressive strength of the cement concrete is measured at 36 MPa, and the flexural tensile strength is recorded as 4.5 MPa. The design institute has put forth two design options for consideration. Scheme 1

entails milling the original asphalt surface layer and laying a new 6 cm asphalt concrete + 2 cm stress-absorbing layer. Scheme 2 entails milling the original asphalt surface layer and laying a new 4 cm asphalt concrete + 2 cm stress-absorbing layer. The asphalt concrete material chosen has a σ_s of 2.87 MPa. The Expressway Group supports Scheme 2 given the project's economic considerations; however, structural design calculations are needed for both schemes.

5.2. Calculation of Cracking at the Bottom of Cement Concrete Slabs

The cumulative number of actions N_e of the design lane standard load can be calculated, as shown in Equation (30):

$$N_e = \frac{N_1 \times \left[(1+g_r)^t - 1\right] \times 365}{g_r} \times \eta = 1.33 \times 10^7 \quad (30)$$

where N_1 is the number of daily actions of the design axile load, taken as 5000 times; g_r is the annual average growth rate of traffic volume; t is the expected service life, taken as 20 years; η is the lateral distribution coefficient of the vehicle wheel track, taken as 0.22.

According to the specifications [15] (the meaning of symbols can be found in reference specifications), two schemes for checking the cracking of cement concrete slab bottom were carried out, and the calculation results are demonstrated in Table 5 (See Supplementary Materials for details):

Table 5. Checking calculation of cracking at the bottom of cement concrete slabs.

Symbol	Unit	Scheme 1	Scheme 2
D_c	MN·m	54.27	54.27
r_g	m	0.99	0.99
σ_{ps}	MPa	1.41	1.41
σ_p	MPa	2.70	2.70
ζ_a	—	1.45	1.45
σ_{psa}	MPa	1.25	1.29
σ_{pma}	MPa	2.39	2.47
k_f	—	2.55	2.55
k_r	—	0.87	0.87
k_c	—	1.15	1.15
σ_{pr}	MPa	3.19	3.29
σ_{pm}	MPa	2.39	2.47
σ_{tr}	MPa	0.18	0.26
σ_{tm}	MPa	0.80	0.92
γ_r	—	1.22	1.22

According to Equations (1) and (2), the verification Scheme 1 is as follows:

$$\gamma_r(\sigma_{pr} + \sigma_{tr}) = 1.22 \times (3.19 + 0.18) = 4.11 \text{ MPa} \leq f_r = 4.5 \text{ MPa} \quad (31)$$

$$\gamma_r(\sigma_{pm} + \sigma_{tm}) = 1.22 \times (2.39 + 0.80) = 3.89 \text{ MPa} \leq f_r = 4.5 \text{ MPa} \quad (32)$$

According to Equations (1) and (2), the verification Scheme 2 is as follows:

$$\gamma_r(\sigma_{pr} + \sigma_{tr}) = 1.22 \times (3.29 + 0.26) = 4.33 \text{ MPa} \leq f_r = 4.5 \text{ MPa} \quad (33)$$

$$\gamma_r(\sigma_{pm} + \sigma_{tm}) = 1.22 \times (2.47 + 0.92) = 4.14 \text{ MPa} \leq f_r = 4.5 \text{ MPa} \quad (34)$$

In summary, both Schemes 1 and 2 have successfully met the requirements in terms of the calculation of bending tensile stress at the bottom of the plate.

5.3. Calculation of Cracking at the Bottom of Asphalt Layer

Utilizing Equations (15)–(19) and (24)–(28), and Ref. [4], two schemes were employed to evaluate the potential cracking of the bottom layer of the asphalt. The resulting calculations are demonstrated in Table 6 (See Supplementary Materials for details):

Table 6. Calculation of cracking at the bottom of asphalt layer.

Symbol	Unit	Scheme 1	Scheme 2
σ_{t0}	MPa	0.682	0.687
$\sigma_x\lceil T\rceil$	MPa	0.053	0.063
σ_{ps0}	MPa	0.313	0.417
k_{1t}	—	0.7	0.7
σ_s	MPa	2.87	2.87
A_a	—	1.0	1.0
A_c	—	1.0	1.0
K_s	—	3.321	3.321

According to Equation (7), verification Scheme 1 is as follows:

$$0.313\ \text{MPa} < \frac{2.87}{3.321} - 0.7 \times (0.682 + 0.053) = 0.350\ \text{MPa} \tag{35}$$

Qualified verification.

According to Equation (7), verification Scheme 2 is as follows:

$$0.417\ \text{MPa} \geq \frac{2.87}{3.321} - 0.7 \times (0.687 + 0.063) = 0.340\ \text{MPa} \tag{36}$$

Unqualified verification.

In summary, both schemes satisfy the requirements for checking the cracking at the bottom of the cement board according to the specifications; however, when evaluating fatigue cracking at the bottom of the asphalt layer, only the asphalt layer thickness in Scheme 1 meets the necessary criteria.

Consequently, based on the design criterion that the comprehensive stress (comprising temperature stress and load stress) at the bottom of the asphalt layer should be lower than the tensile strength of the asphalt mixture, the proposed design method has been implemented in the structural design of the Weixu Expressway.

In addition, the effective thickness method [7], an international approach, was employed to design the overlay plan for the Weixu Expressway. The original cement concrete thickness of the Weixu Expressway measures 28 cm, and the corresponding conversion coefficient obtained from the provided table is 0.7. The conversion coefficient for the base layer is 0.3. Therefore, the effective thickness (h) is 25 cm. The cumulative number of standard load actions on the designed lane of Weixu Expressway during its design service life is 1.33×10^7, the rebound modulus of the soil foundation is 40 MPa, and according to Table 1, the total thickness is determined to be 31 cm, so the thickness of the asphalt layer is 6 cm. Hence, the effective thickness method yields a calculated layer thickness of 6 cm for the overlay plan. However, considering that this thickness obtained for the asphalt layer is relatively low, Scheme 2 should be chosen. With an increased asphalt layer thickness of 8 cm, the pavement structure would be safer and align with the recommended approach mentioned earlier.

To summarize, when traditional cement board cracking is employed as the design indicator, the thickness of the asphalt layer fails to meet the requirements for fatigue cracking at the bottom of the asphalt layer. As a result, it is advisable to consider increasing

the maximum tensile stress at the bottom joint of the asphalt layer as a calculation indicator in the design of composite pavement structures.

6. Conclusions

(1) The influence of the asphalt layer elastic modulus E_1, the asphalt layer thickness h_1, the cement concrete slab elastic modulus E_2, the thickness of the cement concrete slab h_2, the length of cement concrete slab L, and the foundation reaction modulus k on temperature warping stress is analyzed, and the calculation formula is fitted for temperature warping stress.

(2) The influence of the asphalt layer elastic modulus E_1, the asphalt layer thickness h_1, the cement concrete slab elastic modulus E_2, the thickness the of cement concrete slab h_2, the length and width of the cement concrete slab L * B, the foundation reaction modulus k, and the joint width δ is analyzed, and the asphalt layers σ_x and σ_z at the bottom, the interlayer tensile stress σ_y, and the load stress calculation formula is fitted.

(3) This study examined the influence of a stress absorption layer on enhancing the performance of pavement in terms of cracking prevention. Additionally, a formula was developed to calculate the equivalent modulus of the pavement structure, considering the presence of the stress absorption layer. Research suggests that setting a 1 cm stress-absorbing layer is more effective than the maximum tensile stress at the bottom of an asphalt layer without a stress-absorbing layer σ_1 reduced by 69.7%, equivalent stress σ_e decreased by 34.1%, and maximum shear stress τ_{max} decreased by 30.9%.

(4) This study improved the existing design method for composite pavement structures and developed a design method for determining the thickness of the asphalt layer in composite pavement. This method uses the bending tensile stress at the bottom of the slab as the primary control parameter in pavement structural design, while the maximum tensile stress at the joint at the bottom of the asphalt layer serves as a validation parameter. By applying this method to the Weixu Expressway, this study evaluated its effectiveness. The results indicate that both schemes meet the fatigue cracking criteria for the bottom of the cement concrete slab (based on existing standards). However, only Scheme 1 satisfies the cracking criteria for the bottom of the asphalt layer (based on the new method). Consequently, this study recommends Scheme 1 (6 cm AC + 2 cm stress-absorbing layer) as the optimal pavement structure design. However, it should be noted that this study's proposed new pavement structure design method still has some limitations, particularly in the analysis and discussion of fracture mechanics parameters. Addressing these limitations will be a focus of future research.

Supplementary Materials: The following supporting information can be downloaded at: https://www.mdpi.com/article/10.3390/app15041691/s1.

Author Contributions: N.F.: Conceptualization, Methodology, Data curation, Formal analysis, Writing—Review and Editing, Supervision and Funding acquisition; X.W.: Data curation, Writing—Original draft, Formal analysis, Validation, Methodology and Investigation. H.C.: Conceptualization, Resources and Supervision. K.Y.: Project administration, Methodology and Investigation. All authors have read and agreed to the published version of the manuscript.

Funding: This research was funded by the National Natural Science Foundation of China (Grant No.52409041), the Open Research Fund of the State Key Laboratory of Simulation and Regulation of Water Cycle in River Basin (China Institute of Water Resources and Hydropower Research) (Grant NO: IWHR-SKL-KF202412), the Open Research Fund of Key Laboratory of Water Safety for Beijing–Tianjin–Hebei Region of Ministry of Water Resources (Grant NO: IWHR-JJJ-202401), the Program of the Natural Science Foundation of Tianjin (20JCQNJC01320), the Jiangxi Provincial Department of Education Science and Technology Project (GJJ214605), the Tianjin Transportation Science and

Technology Department Plan Project (2024-B02), and the Key Research and Development Program of Tianjin (No. 24YFXTHZ00230).

Institutional Review Board Statement: Not applicable.

Informed Consent Statement: Not applicable.

Data Availability Statement: The original contributions presented in this study are included in the article. Further inquiries can be directed to the corresponding author.

Conflicts of Interest: Author Kang Yu was employed by the company No. 6 Engineering Co., Ltd. of FHEC of CCCC. The remaining authors declare that the research was conducted in the absence of any commercial or financial relationships that could be construed as a potential conflict of interest.

References

1. Kim, J.; Aplicano, B.; Andryanti, D.M.; Park, D.W. Development of mechanistic-empirical design logic for predicting reflective cracking life of composite pavement. *Int. J. Highway Eng.* **2022**, *24*, 29–38. [CrossRef]
2. Zarei, B.; Talebsafa, M.; Shafabakhsh, G.A. Comparative evaluation of dynamic responses of rcc composite pavement under different moving axles. *Can. J. Civ. Eng.* **2023**, *50*, 498–509. [CrossRef]
3. Bryce, J.; Katicha, S.; Flintsch, G.; Diefenderfer, B.K. Developing a network-level structural capacity index for composite pavements. *J. Infrastruct. Syst.* **2016**, *23*, 04016020. [CrossRef]
4. Fang, N.; Li, H.; Li, Q.; Wang, X.; Hu, S.; Xin, L. Study on asphalt layer of composite pavement temperature shrinkage stress considering stress relaxation. *Mater. Struct.* **2021**, *54*, 32. [CrossRef]
5. Luo, Y.; Tian, B.; Niu, K. Numerical analysis of reflective cracking of continuous reinforced composite pavement under multifactor coupling. *Mob. Inf. Syst.* **2021**, *2021*, 7065124. [CrossRef]
6. Wei, F.; Cao, J.; Zhao, H.; Han, B. Laboratory investigation on the interface bonding between portland cement concrete pavement and asphalt overlay. *Math. Probl. Eng.* **2021**, *2021*, 8831287. [CrossRef]
7. Sun, L. *Theory of Structural Behavior of Asphalt Pavement*; Tongji University Press: Shanghai, China, 2003.
8. Sutherland, F.C. American Association of State Highway and Transportation Officials: Current Research Program in Bridges. In Proceedings of the Research Needs for Short- and Medium-Span Bridges, Washington, DC, USA, 17–19 November 1986; The National Academies of Sciences, Engineering, and Medicine: Washington, DC, USA, 1987.
9. Bahia, H.U.; Davies, R. Effect of crumb rubber modifiers (crm) on performance-related properties of asphalt binders. *J. Assoc. Asph. Paving Technol.* **1994**, *63*, 414.
10. Esch, D.C. Construction and Benefits of Rubber-modified Asphalt Pavements. *Transp. Res. Rec.* **1982**, *860*, 5–13.
11. Wei, L. Research on Design Technology of Asphalt Overlay on Cement Concrete Pavement of Urban Roads. Doctoral Dissertation, Chongqing Jiaotong University, Chongqing, China, 1982.
12. Yao, Z. *Highway Design Manual—Pavement*; People's Publishing House: Beijing, China, 1992.
13. Shen, J. *A Summary of Foreign Asphalt Pavement Design Methods*; People's Transportation Publishing House: Beijing, China, 2004.
14. Mateos, A.; Millan, M.A.; Harvey, J.T.; Paniagua, F.; Wu, R. Mechanisms of asphalt cracking and concrete-asphalt debonding in concrete overlay on asphalt pavements. *Constr. Build. Mater.* **2021**, *301*, 124086. [CrossRef]
15. Ministry of Transport of the People's Republic of China (MOT). *Design Code for Cement Concrete Pavement of Highways*; JTG D40; China Transport Press: Beijing, China, 2011.
16. Elseifi, M.; Bandaru, R. *Cost Effective Prevention of Reflective Cracking of Composite Pavement*; Department of Civil and Environmental Engineering: Baton Rouge, LA, USA, 2011. Available online: https://rosap.ntl.bts.gov/view/dot/23332 (accessed on 3 February 2025).
17. Fang, N.; Wang, X.; Ye, H.; Sun, Y.; Yuan, L. Study on fatigue characteristics and interlayer design method of waterproof cohesive bridge deck layer. *Appl. Sci.* **2019**, *9*, 2090. [CrossRef]
18. Jiang, S.; Ding, S. Case analysis of composite base asphalt pavement structure design based on French standards. *J. China Foreign Highw.* **2018**, *38*, 69–72. (In Chinese)
19. Wu, C. Impact fatigue behaviour of gfrp mesh reinforced engineered cementitious composites for runway pavement. *Constr. Build. Mater.* **2019**, *230*, 116898. [CrossRef]
20. Ye, H.; Fang, N.; Wang, X.; Sun, Y. Typical pavement structure optimization in eastern inner mongolia using a combined weight-fuzzy approach. *Int. J. Pavement Res. Technol.* **2022**, *16*, 841–861. [CrossRef]
21. Fang, N.; Chang, H.; Hu, S.; Hao, L.; Meng, Q. Climate Zoning of Asphalt Pavement Based on Spatial Interpolation and Fuzzy C-Means Algorithm. *Int. J. Pavement Eng.* **2022**, *24*, 2072498. [CrossRef]
22. Wang, X.; Fang, N.; Ye, H.; Zhao, J. Fatigue damage analysis of cement-stabilized base under construction loading. *Appl. Sci.* **2018**, *8*, 2263. [CrossRef]

23. Fan, S. Thermo-Dynamic Response and Temperature Fatigue Damage Analysis of Asphalt Pavement Based on Temperature Field/Modulus Field. Doctoral Dissertation, Chongqing Jiaotong University, Chongqing, China, 2024. (In Chinese) [CrossRef]
24. Li, H.; Fang, N.; Wang, X.; Fang, Y.; Li, X.; Li, C.; Ding, S. Load Transfer Efficiency Analysis and Void Evaluation of Composite Pavement Cement Concrete Slab. *Adv. Mater. Sci. Eng.* **2022**, *2022*, 4490485. [CrossRef]
25. Shao, Q. Research on the Expansion of Reflection Cracks in Asphalt Pavement Under Vehicle Temperature Load. Master's Dissertation, Hebei University, Baoding, China, 2024. (In Chinese) [CrossRef]
26. Yuan, J.; Cheng, H.; Sun, L.; Li, J. Causes of arch expansion on semi-rigid base asphalt pavement based on temperature-stress analysis. *China J. Highw. Transp.* **2024**, *37*, 182–196. (In Chinese) [CrossRef]
27. Tang, T.; Zha, X.; Xiao, Q.; Chen, Y. Laboratory characterization and field validation of roadmesh-reinforced asphalt pavement in china. *Int. J. Civ. Eng.* **2016**, *16*, 299–313. [CrossRef]
28. Chen, Y.; Zhang, H.; Quan, L.; Zhang, Z.; Lü, C. Theoretical Assessment on Piezoelectric Energy Harvesting in Smart Self-powered Asphalt Pavements. *J. Vib. Eng. Technol.* **2018**, *6*, 1–10. [CrossRef]
29. Wu, J.; Wu, S. Evaluation of old cement concrete pavement overlay with joints using three-dimensional finite element method. *J. Chang. Univ. (Nat. Sci. Ed.)* **2002**, *1*, 10–13. (In Chinese)

Disclaimer/Publisher's Note: The statements, opinions and data contained in all publications are solely those of the individual author(s) and contributor(s) and not of MDPI and/or the editor(s). MDPI and/or the editor(s) disclaim responsibility for any injury to people or property resulting from any ideas, methods, instructions or products referred to in the content.